Climate-driven deterioration of future ozone pollution in Asia predicted by machine learning with multisource data

Huimin Li[1], Yang Yang[1*], Jianbing Jin[1], Hailong Wang[2], Ke Li[1], Pinya Wang[1], Hong Liao[1]

[1]Jiangsu Key Laboratory of Atmospheric Environment Monitoring and Pollution Control, Jiangsu Collaborative Innovation Center of Atmospheric Environment and Equipment Technology, School of Environmental Science and Engineering, Nanjing University of Information Science and Technology, Nanjing, Jiangsu, China

[2]Atmospheric Sciences and Global Change Division, Pacific Northwest National Laboratory, Richland, Washington, USA

*Correspondence to yang.yang@nuist.edu.cn

Abstract

Ozone (O_3) is a secondary pollutant in the atmosphere formed by photochemical reactions that endangers human health and ecosystems. O_3 has aggravated in Asia in recent decades and will vary in the future. In this study, to quantify the impacts of future climate change on O_3 pollution, near-surface O_3 concentrations over Asia in 2020–2100 are projected using a machine learning (ML) method along with multisource data. The ML model is trained with combined O_3 data from a global atmospheric chemical transport model and real-time observations. The ML model is then used to estimate future O_3 with meteorological fields from multi-model simulations under various climate scenarios. The near-surface O_3 concentrations are projected to increase by 5–20% over South China, Southeast Asia, and South India and less than 10% over North China and Gangetic Plains under the high forcing scenarios in the last decade of 21st century, compared to the first decade of 2020–2100. The O_3 increases are primarily owing to the favorable meteorological conditions for O_3 photochemical formation in most Asian regions. We also find that the summertime O_3 pollution over eastern China will expand from North China to South China and extend into the cold season in a warmer future. Our results demonstrate the important role of climate change penalty on Asian O_3 in the future, which provides implications for environmental and climate strategies of adaptation and mitigation.

1. Introduction

Tropospheric ozone (O_3) is a secondary air pollutant, formed by photochemical oxidation of nonmethane volatile organic compounds (NMVOCs) and carbon monoxide (CO) in the presence of nitrogen oxides (NO_X = NO + NO_2) and sunlight. It has adverse effects on human health (Malley et al., 2017; Cakmak et al., 2018), vegetation growth (Yue et al. 2017; Mills et al., 2018) and climate change (Checa-Garcia et al., 2018; Gaudel et al., 2018). A better understanding of the causes of changes in O_3 concentrations is useful for developing effective environment and climate strategies.

Since mid-1990s, Asian regions, including South Asia, East Asia and Southeast Asia, have experienced the fastest O_3 increase rate of 2–8 ppb/decade at remote surface sites and in the lower free troposphere across the world (IPCC, 2021). A number of air quality monitoring stations have been established in China since 2013 to measure real-time near-surface particulate matter, O_3, and other air pollutants. The measurements showed an increasing trend of urban warm-season daily maximum 8-hour average (MDA8) O_3 concentrations of 2.4 ppb (5%) yr^{-1} that is faster than any other regions worldwide during 2013–2019 (Lu et al., 2020). However, many regions in Asia lack O_3 observations with sufficient spatial and temporal coverage. Also, most of the present regional observations are collected only near population clusters, which are not representative of the entire region (Zhou et al., 2022).

To supplement the limited near-surface O_3 measurements, many studies

utilized global and regional models with comprehensive physical and chemical processes to simulate O_3 concentrations (Zhu et al., 2017; Gao et al., 2020; Yang et al., 2022). Moreover, statistical models have also been used to estimate O_3 concentrations (Chen et al., 2020; Zhang et al., 2020). In recent years, machine learning (ML) approaches, such as random forest (Xue et al., 2020; Wei et al., 2022), neural network (Di et al., 2017), support vector machine (Su et al., 2020), extreme gradient boosting (Liu et al., 2020), and ensemble learning (Liu et al., 2022), were widely applied to estimate O_3 levels based on potential influential factors (e.g., precursor emissions, meteorological conditions, land use, surface elevation, gross domestic product, population density, and geographical variables). The abovementioned previous studies utilizing the ML methods showed high computational efficiency and accuracy, with an overall R^2 between the observed and predicted O_3 concentrations in the range of 0.7–0.9.

Meteorological factors and synoptic conditions play important roles in affecting O_3 pollution (Fu and Tai, 2015; Gong and Liao, 2019; Yin et al., 2019; Liu et al., 2020; Dang et al., 2021). Gong and Liao. (2019) illustrated that hot, dry, and stagnant weather conditions are favorable for the formation and persistence of severe O_3 pollution over northern China. High air temperature along with intense incoming shortwave radiation accelerates both photochemical reaction rates and natural precursor emissions for O_3 production (Jacob and Winner, 2009). Under high relative humidity conditions, O_3

concentrations decrease due to many complex physical and chemical mechanisms (Jeong and Park, 2013; Kavassalis and Murphy., 2017; Lu et al., 2019; Li M. et al., 2021a). Cloud and precipitation impact O_3 levels through reducing the downwelling solar radiation and washout of pollutants (Toh et al., 2013). Anomalous sea level pressure patterns can affect the long-range transport of O_3 by influencing atmospheric circulation (Santurtún et al., 2015). By changing the air stagnant condition and transport of pollutants, wind fields can also affect O_3 concentrations in local and downwind areas of emission sources (Doherty et al., 2013).

Future climate change corresponding to the different climate scenarios can impact O_3 through altering meteorological conditions (Wang et al., 2013, Fu and Tian et al., 2019). Using regional climate fields downscaled from general circulation models to investigate potential O_3 variations in the U.S. due to changing climate, Fann et al. (2015) projected the MDA8 O_3 to increase by 1–5 ppb as daily maximum average temperature increases by 1–4°C in 2030 relative to 2000. Colette et al. (2015) estimated that the climate penalty for future summertime near-surface O_3 reaches 0.99–1.5 ppb by the end of the 21st century (2071–2100) in Europe compared to present-day levels using an ensemble of eight global coupled climate-chemistry models under the RCP (Representative Concentration Pathway) 8.5 scenario. Through fixing sea surface temperature at present-day and future conditions in five atmospheric-only models as part of the AerChemMIP (Aerosol Chemistry Model

Intercomparison Project), Zanis et al. (2022) projected the climate change penalties and benefits on global near-surface O_3 concentrations from 2015 to 2100 under scenarios of Shared Socioeconomic Pathways (SSPs) 3-7.0. They found O_3 reductions in most regions of the globe, except a robust O_3 climate penalty of 1–2 ppb $°C^{-1}$ in South and East Asia under global warming following the SSP3-7.0 pathway. However, SSP3-7.0 is not a good representative scenario for both air quality and climate in Asia. The emissions of greenhouse gases (GHGs) and air pollutants over East Asia in SSP3-7.0 are assumed to significantly increase in the near future and keep at high levels in the middle of the 21st century among all SSPs (Li et al., 2022), while the emissions of air pollutants have been cut by a lot since 2010s in the real world (Wang et al., 2021). The GHGs and pollutant emissions are very likely to continually decline in the future related to the carbon neutrality commitment (Cheng et al., 2021).

In this study, we aim to better characterize the impact from future climate change on Asian O_3 pollution using multiple state-of-the-art modeling tools and data. It is important for policy-makers that mitigating global climate change potentially has positive benefits to surface air quality through meteorological factors, not only the reduction in fossil fuel co-emissions. The near-surface O_3 concentrations covering 2020–2100 in Asia are projected using a ML method integrated with multisource data, including assimilated O_3 data that combine ground observations across China and simulations from a global 3-D chemical transport model (GEOS-Chem), meteorological fields under various climate

scenarios from the latest Coupled Model Intercomparison Project Phase 6 (CMIP6) multi-model simulations, and other auxiliary data (e.g., emissions, land use, topography, population density, and spatiotemporal information). ML approach gives the capacity to explore many scenarios more rapidly and for longer time periods than the chemical transport model process-based modeling. Details of the data and methodology used in this study are described in section 2. Section 3 analyzes the results of climate-driven O_3 variations over different key regions of Asia. Section 4 summarizes the main conclusions and discusses potential uncertainties in this study.

2. Materials and Methods

2.1 GEOS-Chem model description

Figure 1 illustrates the procedures for predicting future near-surface O_3 over Asia under four scenarios. To assimilate O_3 data for the ML model training, the near-surface O_3 concentrations over Asia from 2014 to 2019 are firstly simulated using the nested-grid version of the 3-D GEOS-Chem model (version 12.9.3), driven by the Modern-Era Retrospective analysis for Research and Applications, Version 2 (MERRA-2) reanalysis meteorological data (Gelaro et al., 2017). The nested GEOS-Chem has 47 vertical layers from the surface up to 0.01 hPa, with a horizontal resolution of 0.5° latitude × 0.625° longitude over the Asia domain (11°S–55°N, 60–150°E). The lateral boundaries of chemical tracer concentrations are provided by global simulations at 2° latitude × 2.5° longitude horizontal resolution. The model includes fully coupled aerosol-O_3-

NO_x-hydrocarbon chemical mechanisms (Park et al., 2004; Pye et al., 2009; Mao et al., 2013), with about 300 species participated in over 400 kinetic and photochemical reactions (Bey et al., 2001). The stratospheric O_3 chemistry is simulated through linearized O_3 parameterization scheme (LINOZ; Mclinden et al., 2000), and the planetary boundary layer mixing is calculated by a nonlocal scheme (Lin and McElroy, 2010). GEOS-Chem has shown a good performance in reproducing spatiotemporal distributions of O_3 concentrations (e.g., Ni et al., 2018; Li et al., 2019).

The historical (2014–2019) anthropogenic emissions of O_3 precursor gases, including NO_x, NMVOCs, and CO, utilized in the nested domain are obtained from the Community Emissions Data System (CEDS; Hoesly et al., 2018) version 2021_04_21, which fully considered the recent emission reductions in China related to clean air measures. The biomass burning emissions are acquired from the Global Fire Emissions Database version 4 (GFED4; van der Werf et al., 2017). Biogenic emissions of NMVOCs from the Model of Emissions of Gases and Aerosols from Nature (MEGAN) version 2.1 are employed, with updates from Guenther et al. (2012). Soil NO_x sources are calculated with an updated version of the Berkeley-Dalhousie Soil NO_x Parameterization scheme (Hudman et al., 2012). NO_x emissions from lightning are as described by Murray et al. (2012), and the vertical distribution of emissions follows Ott et al. (2010).

2.2 Ground O_3 observations

To improve the performance of the ML model in predicting O_3 concentrations, the nationwide hourly near-surface O_3 concentrations in China during 2014–2019 are obtained from the China Ministry of Ecology and Environment (MEE) and used for O_3 data assimilation, which has been widely used to examine pollution over China in previous studies (Li K. et al., 2020, 2021; Qian et al., 2022). The observational network had about 500 monitoring sites in 2013, and expanded to more than 1500 sites after 2019, covering 360 cities in mainland China. In this study, the quality controlled hourly O_3 observations in 360 cities are averaged within each 0.5° latitude × 0.625° longitude grid of the GEOS-Chem model.

2.3 Data assimilation

The assimilation system, which is used to combine the O_3 observations across China with results from GEOS-Chem simulations, is based on a three-dimensional variational (3DVar) data assimilation (Kalnay, 2003; Evensen et al., 2022). The goal of the 3DVar is to find the maximum likelihood estimation of a state vector x, which is the O_3 concentrations here in this study, given the available observations y through minimizing the cost function:

$$J(x) = \frac{1}{2}(\boldsymbol{x} - \boldsymbol{x}^b)^{\mathrm{T}}\,\mathbf{B^{-1}}\,(\boldsymbol{x} - \boldsymbol{x}^b) + \frac{1}{2}(\boldsymbol{y} - \mathrm{H}(\boldsymbol{x}))^{\mathrm{T}}\,\mathbf{O^{-1}}\,(\boldsymbol{y} - \mathrm{H}(\boldsymbol{x}))$$

Here $\boldsymbol{x}^b$ represents the priori simulation. **B** is the empirical background covariance matrix formulated as a product of the uncertainty in the simulated value and a distance-based correlation matrix **C**, and the individual element is calculated as:

$$\mathbf{B}_{i,j} = 0.2 * \boldsymbol{x}_i^b * 0.2 * \boldsymbol{x}_j^b * \mathbf{C}_{i,j}$$

Here we have used 20% choice to characterize uncertainty of the O_3 simulation, the correlation matrix is empirically set as:

$$\mathbf{C}_{i,j} = e^{-(\frac{d_{i,j}}{200km})^2/2}$$

Here $d_{i,j}$ represents the spatial distance between the grid cell i and j.

H denotes the linear observation operator that converts the simulation results into the observational space. Here all observations are assumed to be independent, and therefore **O** is a diagonal covariance matrix storing the square of the observation uncertainty, which is also set as 20% similarly.

Comparisons between observed and assimilated O_3 concentrations over 2014–2019 are shown in Figure 2. The overall correlation coefficient (R) is 0.94, and the normalized mean bias (NMB) is –0.1%, suggesting that the assimilated data have an excellent representation of O_3 observations and minimize the uncertainties of GEOS-Chem simulations in China.

2.4 Predicting O_3 using a machine learning method

In this study, a random forest (RF) model is used to predict O_3 concentrations, similar to our previous studies (Li H. et al., 2021, 2022), with input data of assimilated O_3 concentrations in China that combine observations and results from GEOS-Chem model simulations, GEOS-Chem simulated O_3 concentrations outside of China, MERRA-2 meteorological variables, O_3 precursor emissions, land cover (LC), normalized difference vegetation index (NDVI), topography (TOPO), population density (POP), and the month of the

year (MOY) and geographic location of each model grid as spatiotemporal information. Details of the datasets are summarized in Table 1.

For predicting future climate-driven near-surface O_3 concentrations, the ML model is trained with samples over 2014–2018 and the remaining 2019 data are used for model validation. To obtain an optimal ML model, hyperparameters are firstly tuned using the 10-fold cross-validation (Rodriguez et al., 2010). The best hyperparameters (n_estimators=200, min_samples_split=2, max_features= "sqrt", bootstrap= "True") of the ML model are utilized. Several statistical metrics, including coefficient of determination (R^2), mean absolute error (MAE), root mean square error (RMSE) and mean relative error (MRE) are used to evaluate the performance of ML model. Then the climate-driven near-surface O_3 concentrations during 2020–2100 under four SSPs (SSP1-2.6, SSP2-4.5, SSP3-7.0 and SSP5-8.5) in Asia can be estimated using the trained ML model with varying meteorological factors under the climate change scenarios. Both anthropogenic and natural emissions of O_3 precursors are fixed at the present-day levels for the prediction.

2.5 Meteorological fields from CMIP6 multi-model simulations

Monthly meteorological parameters under four different future climate scenarios, including SSP1-2.6, SSP2-4.5, SSP3-7.0 and SSP5-8.5 (a representation of low, intermediate, medium to high, and high forcing levels, respectively), are fed to a ML model to predict near-surface O_3 concentrations. The Scenario Model Intercomparison Project (ScenarioMIP) as part of CMIP6

239 provides multi-model projections of climate variables driven by future emission
240 and land use changes under different SSPs (O'Neill et al., 2016). In our study,
241 meteorological fields, such as air temperature (at 2m, 850 hPa, and 500 hPa),
242 wind fields (at 850 and 500 hPa), surface relative humidity, incoming shortwave
243 radiation at the surface, total cloud cover, precipitation rate, and sea level
244 pressure, are chosen as the key meteorological predictors for near-surface O_3
245 concentrations, which are obtained from 18 global climate models, i.e.,
246 ACCESS-CM2, ACCESS-ESM1-5, CanESM5, CESM2-WACCM, CMCC-CM2-
247 SR5, EC-Earth3-Veg, EC-Earth3, FGOALS-f3-L, FGOALS-g3, GFDL-ESM4,
248 INM-CM5-0, IPSL-CM6A-LR, MIROC6, MPI-ESM1-2-HR, MPI-ESM1-2-LR,
249 MRI-ESM2-0, NorESM2-LM, and NorESM2-MM. Before being applied to the
250 ML model, future meteorological fields from ScenarioMIP are adjusted by their
251 potential bias, characterized as the difference in their historical climatological
252 mean (2014–2019) and MERRA-2 following Li et al. (2022). It minimizes the
253 inconsistencies in the initial conditions in models and reanalysis data.

254 **3. Results**

255 **3.1 Predictive capability of the machine learning model**

256 The predicted monthly O_3 concentrations over Asia in 2019 by the ML
257 model are in good agreement with the assimilated O_3 data constructed with
258 observations and GEOS-Chem model results (Fig. 3). The overall R^2 between
259 the predicted and assimilated O_3 concentrations is as high as 0.92 and the ML
260 model has a low MRE of 9% in predicting O_3 concentrations over the Asia

domain. Overall, these statistical indices indicate that the RF model is promising for predicting the spatial distributions and temporal variations of near-surface O_3 concentrations over Asia, which can provide a practical means for studying long-term variations in O_3 under the future climate change.

Meanwhile, the ML model predictive capability for each grid cell over the entire domain during 2014–2019 is further evaluated and demonstrated in Figure 4. Regarding the spatial performance, the estimated O_3 concentrations are highly correlated to the assimilated data in most regions of Asia with small biases, indicating a strong spatial predictive ability of the RF model. More than 80% of land areas have a R^2 greater than 0.9. In terms of model uncertainties, about 95% of land areas have a RMSE (MAE) less than 3 (2) parts per billion (ppb). Furthermore, approximately 86% of land areas show small modeling bias with MRE below 5%. Note that several grid cells show MRE over 5% but still below 15%, which is related to the data assimilation using monitored and simulated O_3 concentrations in China and the coarse resolution for coastal areas and islands over Southeast Asia.

Figure 5 shows the importance score of independent variables that contribute to the prediction of trained ML model, which called Gini importance and implies the influence of input features on the target variable in the ML model. The results suggest that among all the input predictors, relative humidity, incoming solar radiation at the surface, and topography are the top-three most influential variables for the model construction of near-surface O_3 in Asia, with

283 importance scores of 15%, 12% and 10%, respectively. The primary importance
284 of relative humidity has also been reported in previous studies (e.g., Han et al.,
285 2020; Qian et al., 2022). Other meteorological parameters, such as cloud cover,
286 sea level pressure, air temperature, precipitation, also have a substantial
287 impact on the O_3 estimates, with importance scores ranging from 4% to 8%. In
288 the ML model, the emissions of three primary O_3 precursors, including NMVOCs,
289 NO_x, and CO, have a relatively low importance score of 4–5% individually due
290 to the spatiotemporal diversity of O_3 production regimes. However, it is noted
291 that the O_3 variations in different regions are dominated by different
292 meteorological factors (Weng et al., 2022). The importance score of each
293 independent feature quantified in this study can only reflect the overall
294 importance across Asia, which is less representative of any specific regions.

295 **3.2 Predicted future climate-driven O_3 variations**

296 Figure 6 shows the predicted absolute and percentage changes in annual
297 mean near-surface O_3 concentrations in response to climate change between
298 the first and last decades of 2020–2100 based on the future meteorological
299 fields from the 18 CMIP6 models. Fig. 7 shows the time series of the regional
300 averaged values over six sub-regions of Asia during 2020–2100. Under the
301 global warming trends of all future scenarios, the climate-driven near-surface
302 O_3 concentrations increase constantly from 2020 to 2100 over many key
303 regions in Asia, such as North China (NC), South China (SC), Southeast Asia
304 (SEA), South India (SI) and Gangetic Plains (GP), except the Tibetan Plateau

(TP). The O_3 concentrations over SC, SEA, and SI are projected to increase considerably with the maximum increase up to 5 ppb (20%) in 2095 (2091–2100 mean) compared to 2025 (2020–2029 mean) under the SSP5-8.5 scenario, revealing a strong O_3-climate penalty in most Asian regions. The climate-driven changes in O_3 concentrations are smaller under the less warming scenarios, especially in SSP1-2.6 that has O_3 changes less than 5% across Asia. These suggest that future climate following low emissions and sustainable pathways is more favorable for the mitigation of O_3 pollution in Asia than high forcing scenarios.

The strong O_3-climate penalty over eastern China can be attributed to the particularly high O_3 precursor emissions (Fig. S1), relative to western China, which lead to a positive local net O_3 production close to sources in a warming climate (Fig. S2) (Zanis et al., 2022). The absolute and percentage changes in regional averaged near-surface O_3 concentrations between 2025 and 2095 under the four scenarios are shown in Figure 8. The climate-driven changes in O_3 concentrations are gradually stronger from north (2–3%) to south (3–8%) of China, which demonstrates that the changes in meteorology exert a greater impact on near-surface O_3 concentrations over SC than NC under future climate change. By the end of the 21st century, the relative humidity will decrease (Fig. S3) and downward solar radiation will increase (Fig. S4) over SC compared to those in 2025, which are conducive to the O_3 productions, while NC has the opposite changes. Moreover, cloud cover will decrease more over SC than NC

(Fig. S5), contributing to the larger increase in O_3 productions and concentrations over SC than NC in a warming climate.

In South Asia, climate change also enhances O_3 concentrations by <5% over GP and SI (Fig. 8), due to the massive precursor emissions (Fig. S1) and O_3 productions. Over SI, the decreases in relative humidity (Fig. S3) and cloud amount (Fig. S5), and increases in downward solar radiation at the surface (Fig. S4) favor photochemical production of O_3 and induce the large increases in O_3 concentrations in this region. Averaged over SEA, O_3 concentrations driven by higher temperature (Fig. S2), more downward solar radiation (Fig. S4), and lower relative humidity (Fig. S3) and cloud cover (Fig. S5) in 2095 are projected to increase O_3 concentrations by 5–7% in SSP3-7.0 and SSP5-8.5 and 0–3% in SSP1-2.6 and SSP2-4.5 scenarios, relative to 2025 (Fig. 8).

The Tibetan Plateau (TP), known as the highest topography in China with more solar radiation at the surface, has strong stratosphere-troposphere exchanges of O_3 compared with other regions leading to high O_3 concentrations over this region (Fig. S6). Climate-driven O_3 concentrations are projected to decline by less than 2% over TP from 2025 to 2095 (Fig. 8). It is likely because less solar radiation (Fig. S4) and more frequent occurrence of rainy weather (Fig. S7) in the future would reduce the local chemical production of O_3.

3.3 The seasonality of future climate-driven O_3 variations

Climate over Asia has obvious seasonal variation related to the Asian monsoon system. Figure 9 shows the spatial distributions of percentage

changes in projected climate-driven O_3 concentrations in spring (March–April–May, MAM), summer (June–July–August, JJA), autumn (September–October–November, SON), and winter (December–January–February, DJF) between 2025 and 2095 under the four scenarios. In general, air quality in many regions of Asia will deteriorate in all seasons associated with intensified O_3 pollution under climate change.

In eastern China, O_3 pollution occurs most frequently in summer and is more severe in NC than SC currently (Li et al., 2019). Under future climate warming, JJA O_3 concentrations will increase by 5–20% in SC under the high forcing scenarios, while the changes in NC are less than 5%. It suggests that future climate change will expand the summertime O_3 pollution from NC to SC over eastern China. Another feature is the strong increases in O_3 concentrations by 10–20% throughout eastern China and exceeding 20% over Sichuan Basin in SON, which relate to the significant increases in temperature (Fig. S8) and solar radiation (Fig. S9) in this season over central-eastern China under the high forcing scenarios. It further indicates that future climate change will extend the O_3 pollution from summer into autumn.

In South Asia, the climate-driven increases in O_3 concentrations vary from JJA over SI to DJF over GP. Relative to 2025, in summer of 2095, anomalous high pressure (Fig. S10) along with anticyclone (Figs. S11 and S12) dominates South Asia, which is not conducive to O_3 diffusion, leading to increases in JJA O_3 concentrations over SI. The intensified O_3 pollution across GP in DJF under

climate change is related to the strong surface warming (Fig. S8), decreases in relative humidity (Fig. S13), cloud cover (Fig. S14) and rainfall (Fig. S15), as well as increases in solar radiation at the surface (Fig. S9), favoring the photochemical production of O_3. In north part of Southeast Asia, JJA has the largest O_3 rise via the same mechanism as for SI, while O_3 increases by the same magnitude in all seasons in south part of Southeast Asia driven by future climate change.

4. Conclusions and discussion

The O_3 pollution has been increasing over Asia in recent decades, which harms human health and vegetations. In the future warmer climate, O_3 pollution over Asia can be modulated by changes in meteorological fields. In this study, to examine the variations in O_3 concentrations over Asia due to the future climate change, monthly near-surface O_3 concentrations from 2020 to 2100 under four climate scenarios (SSP1-2.6, SSP2-4.5, SSP3-7.0, and SSP5-8.5) are predicted using a ML model with input data from assimilated O_3 combining GEOS-Chem simulations and real-time observations, future meteorological parameters from CMIP6 multi-model simulations, emissions of O_3 precursors, land use, topography, population density and spatiotemporal information. Our results suggest that the future O_3 pollution over Asia will be significantly exacerbated in a warming climate, especially under high forcing scenarios.

Trained by the assimilated O_3 concentrations and reanalysis data, the ML model can well predict O_3 over Asia with the coefficient determination of 0.92

between assimilated and predicted O_3 concentrations and relative error of 9%. Then the future Asian O_3 concentrations from 2020 to 2100 driven by climate change are projected in the ML model with varying meteorological fields from 18 CMIP6 models under four future climate scenarios.

The climate penalty on O_3 is robust over most regions of Asia. The annual mean O_3 levels in 2095 are projected to increase by 5–20% relative to 2025 under the high forcing scenarios over South China, Southeast Asia, and South India and less than 10% over North China and Gangetic Plains, due to more favorable meteorological conditions for O_3 photochemical production, while there is a decrease of <5% over the Tibetan Plateau. The climate-driven changes in O_3 concentrations are smaller under the less warming scenarios, suggesting that future climate following low emissions and sustainable pathways would be more effective in the mitigation of O_3 pollution in Asia than the high forcing scenarios. Seasonal variation analysis reveals that the summertime O_3 pollution over eastern China will expand from North China to South China and extend into the cold season under the future climate change. In addition, South Asian O_3 pollution will increase over South India in summer and over Gangetic Plains in winter.

Zanis et al. (2022) analyzed the global climate change benefit and penalty on O_3 based on sensitivity simulations from five CMIP6 models under the SSP3-7.0 scenario. They showed positive changes in JJA O_3 concentrations by less than 1 ppb from 2010 to 2095 over East Asia and South Asia driven by climate

change, but with large uncertainties due to the model diversity. The ML method in this study gives similar positive changes in O_3 as Zanis et al. (2022). Pommier et al. (2018) applied the EMEP chemical transport model driven by the downscaled meteorological data from the NorESM1-M to investigate the impacts of regional climate change on near-surface O_3 over India. They showed that near-surface O_3 would increase by up to 4% over Northern India and decrease by 3% over Southern India from 2050 to 2100 under the RCP8.5 scenario. We show that the climate-driven O_3 in this study would increase over both Gangetic Plains (0.2%) and South India (3%) under the SSP5-8.5 scenario in 2050 relative to 2016 (2014–2019 mean). The discrepancies may rise from that the results of Pommier et al. (2018) were based on NorESM1-M simulated climate alone, while the climate change predicted by 18 CMIP6 models were applied in this study and the ensemble mean O_3 concentrations were shown here.

There are a few uncertainties and limitations in the projected near-surface O_3 concentrations over Asia in terms of input data, GEOS-Chem simulations, CMIP6 multi-model simulations, and the ML model. First, only observational data over 2014–2019 across China were used for the O_3 assimilation. Longer-term measurements with broader spatial coverage are more desirable to improve the model performance. Land use data and population density are fixed at present-day conditions when predicting the future O_3 since we focus on the variations in meteorological parameters under climate change, which will

vary in the future. In addition, natural O_3 precursor emissions such as biogenic emissions of NMVOCs, and NO_x from soil and lightning sources are fixed at year-2016 levels in the future estimates, which can induce biases in the O_3 projections since climate change can strongly influence natural emissions of O_3 precursors (Liu et al., 2019). Although the methane concentrations in GEOS-Chem model are prescribed and its role in the O_3 production is not considered in the ML model, the climate influence of methane is included in the CMIP6 multi-model simulations. Consequently, the impact of future changes in methane on O_3 concentrations via climate change are considered in the future projections.

Second, the GEOS-Chem model has been demonstrated to well capture the magnitude of and spatiotemporal variations in O_3, with an average bias of about 10% over China (Lou et al., 2014) and Southeast Asia (Marvin et al., 2021), and less than 20% over India (David et al., 2019). The future decrease in relative humidity will cause stomatal closure and also increase near-surface O_3. The O_3-vegetation interactions are not represented in the default GEOS-Chem model. A newly coupled global atmospheric chemistry-vegetation model (Lei et., 2020) could be applied in the future study.

Third, the meteorological parameters characterizing future climate change from the CMIP6 multi-model simulations can also give rise to uncertainties in this study (Xu et al., 2021). Moreover, the spatial autocorrelation in random split of training data for cross-validation would lead to the overly optimistic statistics

of ML model predictive power (Ploton et al., 2020). Additionally, the overall importance scores of the features in this study can only reflect that from the whole study domain. Further investigations are required to identify and quantify the importance score of each local variable contributed to the near-surface O_3 predictions in different specific regions. Also, the good ability of the ML model for the present-day condition may not imply a satisfactorily extrapolation under the future warming condition, which can bias our results and deserves further investigation in future studies.

Last but not least, the near-surface O_3 have increased rapidly in China since 2013 owing to both precursor emission changes and atmospheric warming (Li M. et al., 2021b), which significantly affect human health (Lu et al., 2020) and also requires further studies.

Overall, our study provides a framework of combining real-time observations, chemical transport model simulations and multi-climate model predictions with data assimilation and machine learning methods to estimate future climate driven near-surface O_3 concentrations. The emphasis of this work is to quantify the impacts of future climate change on O_3 pollution in Asia, which is of great significance for the future O_3 pollution mitigation strategies.

Author contributions

YY designed the research. HL performed the model simulations, analyzed data and wrote the initial draft. JJ designed the data assimilation. YY, JJ, HW, and KL helped edit and review the manuscript. All the authors discussed the results and contributed to the final manuscript.

Code and data availability

The GEOS-Chem model is available at https://zenodo.org/record/3974569#.YTD81NMzagR (last access: 1 August 2022). MERRA-2 reanalysis data can be downloaded at https://gmao.gsfc.nasa.gov/reanalysis/MERRA-2/ (last access: 1 August 2022). Multi-model projections of climate variables are from Scenario Model Intercomparison Project in Phase 6 of the Coupled Model Intercomparison Project https://esgf-node.llnl.gov/search/cmip6/ (last access: 1 August 2022). Land cover is derived from http://maps.elie.ucl.ac.be/CCI/viewer/download.php (last access: 1 August 2022). Hourly O_3 concentrations are obtained from the public website of the China Ministry of Ecology and Environment https://www.mee.gov.cn (last access: 1 August 2022). Normalized difference vegetation index is obtained from https://www.ncei.noaa.gov/data/avhrr-land-normalized-difference-vegetation-index/access/ (last access: 1 August 2022). Topography is collected from https://cgiarcsi.community/data/srtm-90m-digital-elevation-database-v4-1/ (last access: 1 August 2022). Population density is

acquired from https://landscan.ornl.gov/landscan-datasets (last access: 1 August 2022).

Acknowledgments

H.W. acknowledges the support by the U.S. Department of Energy (DOE), Office of Science, Office of Biological and Environmental Research (BER), as part of the Earth and Environmental System Modeling program. The Pacific Northwest National Laboratory (PNNL) is operated for DOE by the Battelle Memorial Institute under contract DE-AC05-76RLO1830. The projected O_3 concentrations in this study are available upon request.

Competing Interest

The contact author has declared that neither they nor their co-authors have any competing interests.

Financial support.

This study was supported by the National Key Research and Development Program of China (grant 2019YFA0606800 and 2020YFA0607803) and the National Natural Science Foundation of China (grant 41975159) and Jiangsu Science Fund for Distinguished Young Scholars (grant BK20211541).

Reference

Bey, I., Jacob, D. J., Yantosca, R. M., Logan, J. A., Field, B. D., Fiore, A. M., Li, Q., Liu, H., Mickley, L. J., and Schultz, M. G.: Global modeling of tropospheric chemistry with assimilated meteorology: Model description and evaluation, J. Geophys. Res. Atmos., 106, 23073–23095, https://doi.org/10.1029/2001JD000807, 2001.

Cakmak, S., Hebbern, C., Pinault, L., Lavigne, E., Vanos, J., Crouse, D. L., and Tjepkema, M.: Associations between long-term $PM_{2.5}$ and ozone exposure and mortality in the Canadian Census Health and Environment Cohort (CANCHEC), by spatial synoptic classification zone, Environ. Int., 111, 200–211, https://doi.org/10.1016/j.envint.2017.11.030, 2018.

Checa-Garcia, R., Hegglin, M. I., Kinnison, D., Plummer, D. A., and Shine, K. P.: Historical tropospheric and stratospheric ozone radiative forcing using the CMIP6 database, Geophys. Res. Lett., 45, 3264–3273, https://doi.org/10.1002/2017GL076770, 2018.

Chen, L., Liang, S., Li, X., Mao, J., Gao, S., Zhang, H., Sun, Y., Vedal, S., Bai, Z., Ma, Z., Haiyu., and Azzi, M.: A hybrid approach to estimating long-term and short-term exposure levels of ozone at the national scale in China using land use regression and Bayesian maximum entropy, Sci. Total Environ., 752, 141780, https://doi.org/10.1016/j.scitotenv.2020.141780, 2020.

Cheng, J., Tong, D., Zhang, Q., Liu, Y., Lei, Y., Yan, G., Yan, L., Yu, S., Cui, R. Y., Clarke, L., Geng, G., Zheng, B., Zhang, X., Davis, S. J., and He, K.: Pathways of China's $PM_{2.5}$ air quality 2015−2060 in the context of carbon neutrality, Natl. Sci. Rev., 8, nwab078, https://doi.org/10.1093/nsr/nwab078, 2021.

Colette, A., Andersson, C., Baklanov, A., Bessagnet, B., Brandt, J., Christensen, J. H., Doherty, R., Engardt, M., Geels, C., Giannakopoulos, C., Hedegaard, G. B., Katragkou, E., Langner, J., Lei, H., Manders, A., Melas, D., Meleux, F., Rouïl, L., Sofiev, M., Soares, J., Stevenson, D. S., Tombrou-Tzella, M., Varotsos, K. V., and Young, P.: Is the ozone climate penalty robust in Europe? Environ. Res. Lett., 10, 084015, http://dx.doi.org/10.1088/1748-9326/10/8/084, 2015.

Dang, R., Liao, H., and Fu, Y.: Quantifying the anthropogenic and meteorological influences on summertime surface ozone in China over 2012–2017, Sci. Total Environ., 754, 142394, https://doi.org/10.1016/j.scitot, 2021.

David, L. M., Ravishankara, A., Brewer, J. F., Sauvage, B., Thouret, V., Venkataramani, S., and Sinha, V.: Tropospheric ozone over the Indian subcontinent from 2000 to 2015: Data set and simulation using GEOS-Chem chemical transport model, Atmos. Environ., 219, 117039, https://doi.org/10.1016/j.atmosenv.2019.117039, 2019.

Di, Q., Rowland, S., Koutrakis, P., and Schwartz, J.: A hybrid model for spatially and temporally resolved ozone exposures in the continental United States, J. Air Waste Manage. Assoc., 67, 39–52, https://doi.org/10.1080/10962247.2016.1200159, 2017.

Doherty, R. M., Wild, O., Shindell, D. T., Zeng, G., MacKenzie, I. A., Collins, W. J., Fiore, A. M., Stevenson, D. S., Dentener, F. J., Schultz, M. G., Hess, P., Derwent, R. G., and Keating, T. J.: Impacts of climate change on surface ozone and intercontinental ozone pollution: A multi-model study, J. Geophys. Res., 118, 3744–3763, https://doi.org/10.1002/jgrd.50266, 2013.

Evensen, G., Vossepoel, F. C., and van Leeuwen, P. J.: Data Assimilation Fundamentals: A Unified Formulation of the State and Parameter Estimation Problem, Springer Nature, https://doi.org/10.1007/978-3-030-96709-3, 2022.

Fann, N., Nolte, C. G., Dolwick, P., Spero, T. L., Brown, A. C., Phillips, S., and Anenberg, S.: The geographic distribution and economic value of climate change-related ozone health impacts in the United States in 2030, J. Air Waste Manag. Assoc., 65, 570–580, https://doi.org/10.1080/10962247.2014.996270, 2015.

Fu, T.-M., and Tian, H.: Climate Change Penalty to Ozone Air Quality: Review of Current Understandings and Knowledge Gaps, Curr. Pollut. Rep., 5, 159–171, https://doi.org/10.1007/s40726-019-00115-6, 2019.

Fu, Y., and Tai, A. P. K.: Impact of climate and land cover changes on tropospheric ozone air quality and public health in East Asia between 1980 and 2010, Atmos. Chem. Phys., 15, 10093–10106, https://doi.org/10.5194/acp-15-10093-2015, 2015.

Gao, M., Gao, J., Zhu, B., Kumar, R., Lu, X., Song, S., Zhang, Y., Jia, B., Wang, P., Beig, G., Hu, J., Ying, Q., Zhang, H., Sherman, P., and McElroy, M. B.: Ozone pollution over China and India: seasonality and sources, Atmos. Chem. Phys., 20, 4399–4414, https://doi.org/10.5194/acp-20-4399-2020, 2020.

Gaudel, A., Cooper, O. R., Ancellet, G., Barret, B., Boynard, A., Burrows, J. P.,

Clerbaux, C., Coheur, P. F., Cuesta, J., Cuevas, E., Doniki, S., Dufour, G., Ebojie, F., Foret, G., Garcia, O., Granados-Muñoz, M. J., Hannigan, J. W., Hase, F., Hassler, B., Huang, G., Hurtmans, D., Jaffe, D., Jones, N., Kalabokas, P., Kerridge, B., Kulawik, S., Latter, B., Leblanc, T., Le Flochmoën, E., Lin, W., Liu, J., Liu, X., Mahieu, E., McClure-Begley, A., Neu, J. L., Osman, M., Palm, M., Petetin, H., Petropavlovskikh, I., Querel, R., Rahpoe, N., Rozanov, A., Schultz, M. G., Schwab, J., Siddans, R., Smale, D., Steinbacher, M., Tanimoto, H., Tarasick, D. W., Thouret, V., Thompson, A. M., Trickl, T., Weatherhead, E., Wespes, C., Worden, H. M., Vigouroux, C., Xu, X., Zeng, G., and Ziemke, J.: Tropospheric Ozone Assessment Report: Present-day distribution and trends of tropospheric ozone relevant to climate and global atmospheric chemistry model evaluation, Elem. Sci. Anth., 6, 39, https://doi.org/10.1525/elementa.291, 2018.

Gelaro, R., McCarty, W., Suárez, M. J., Todling, R., Molod, A., Takacs, L., Randles, C. A., Darmenov, A., Bosilovich, M. G., Reichle, R., Wargan, K., Coy, L., Cullather, R., Draper, C., Akella, S., Buchard, V., Conaty, A., da Silva, A. M., Gu, W., Kim, G.-K., Koster, R., Lucchesi, R., Merkova, D., Nielsen, J. E., Partyka, G., Pawson, S., Putman, W., Rienecker, M., Schubert, S. D., Sienkiewicz, M., and Zhao, B.: The Modern-Era Retrospective Analysis for Research and Applications, Version 2 (MERRA-2), J. Clim., 30, 5419−5454, https://doi.org/10.1175/JCLI-D-16-0758.1, 2017.

Gong, C., and Liao, H.: A typical weather pattern for ozone pollution events in North China, Atmos. Chem. Phys., 19, 13725–13740, https://doi.org/10.5194/acp-19-13725-2019, 2019.

Guenther, A. B., Jiang, X., Heald, C. L., Sakulyanontvittaya, T., Duhl, T., Emmons, L. K., and Wang, X.: The Model of Emissions of Gases and Aerosols from Nature version 2.1 (MEGAN2.1): an extended and updated framework for modeling biogenic emissions, Geosci. Model Dev., 5, 1471–1492, https://doi.org/10.5194/gmd-5-1471-2012, 2012.

Han, H., Liu, J., Shu, L., Wang, T., and Yuan, H.: Local and synoptic meteorological influences on daily variability in summertime surface ozone in eastern China, Atmos. Chem. Phys., 20, 203–222, https://doi.org/10.5194/acp-20-203-2020, 2020.

Hoesly, R. M., Smith, S. J., Feng, L., Klimont, Z., Janssens-Maenhout, G., Pitkanen, T., Seibert, J. J., Vu, L., Andres, R. J., Bolt, R. M., Bond, T. C., Dawidowski, L., Kholod, N., Kurokawa, J.-I., Li, M., Liu, L., Lu, Z., Moura, M. C. P., O'Rourke, P. R., and Zhang, Q.: Historical (1750–2014)

anthropogenic emissions of reactive gases and aerosols from the Community Emissions Data System (CEDS), Geosci. Model Dev., 11, 369−408, https://doi.org/10.5194/gmd-11-369-2018, 2018.

Hudman, R. C., Moore, N. E., Mebust, A. K., Martin, R. V., Russell, A. R., Valin, L. C., and Cohen, R. C.: Steps towards a mechanistic model of global soil nitric oxide emissions: implementation and space based-constraints, Atmos. Chem. Phys., 12, 7779–7795, https://doi.org/10.5194/acp-12-7779-2012, 2012.

IPCC: Climate change 2021: The physical science basis. Contribution of working group I to the sixth assessment report of the intergovernmental panel on climate change. Cambridge, UK: Cambridge University Press, 2021.

Jacob, D. J., and Winner, D. A.: Effect of climate change on air quality, Atmos. Environ., 43, 51–63, https://doi.org/10.1016/j.atmosenv.2008.09.051, 2009.

Jeong, J. I., and Park, R. J.: Effects of the meteorological variability on regional air quality in East Asia, Atmos. Environ., 69, 46–55, https://doi.org/10.1016/J.Atmosenv.2012.11.061, 2013.

Kalnay, E.: Atmospheric Modeling, Data Assimilation and Predictability, Cambridge University Press, Cambridge, United Kingdom, 2003.

Kavassalis, S. C., and Murphy, J. G.: Understanding ozone-meteorology correlations: A role for dry deposition, Geophys. Res. Lett., 44, 2922–2931, https://doi.org/10.1002/2016gl071791, 2017.

Lei, Y., Yue, X., Liao, H., Gong, C., and Zhang, L.: Implementation of Yale Interactive terrestrial Biosphere model v1.0 into GEOS-Chem v12.0.0: a tool for biosphere– chemistry interactions, Geosci. Model Dev., 13, 1137–1153, https://doi.org/10.5194/gmd-13-1137-2020, 2020.

Li, H., Yang, Y., Wang, H., Li, B., Wang, P., Li, J., and Liao, H.: Constructing a spatiotemporally coherent long-term $PM_{2.5}$ concentration dataset over China during 1980–2019 using a machine learning approach, Sci. Total Environ., 765, 144263, https://doi.org/10.1016/j.scitotenv.2020.144263, 2021.

Li, H., Yang, Y., Wang, H., Wang, P., Yue, X., and Liao, H.: Projected Aerosol Changes Driven by Emissions and Climate Change Using a Machine Learning Method, Environ. Sci. Technol., 56, 7, 3884–3893, https://doi.org/10.1021/acs.est.1c04380, 2022.

Li, K., Jacob, D. J., Liao, H., Shen, L., Zhang, Q., and Bates, K. H.: Anthropogenic Drivers of 2013–2017 Trends in Summer Surface Ozone in China, P. Natl. Acad. Sci. USA., 116, 422–427, https://doi.org/10.1073/pnas.1812168116, 2019.

Li, K., Jacob, D. J., Shen, L., Lu, X., De Smedt, I., and Liao, H.: Increases in surface ozone pollution in China from 2013 to 2019: anthropogenic and meteorological influences, Atmos. Chem. Phys., 20, 11423–11433, https://doi.org/10.5194/acp-20-11423-2020, 2020.

Li, K., Jacob, D. J., Liao, H., Qiu, Y., Shen, L., Zhai, S., Bates, K. H., Sulprizio, M. P., Song, S., Lu, X., Zhang, Q., Zheng, B., Zhang, Y., Zhang, J., Lee, H. C., and Kuk, S. K.: Ozone pollution in the North China Plain spreading into the late-winter haze season, P. Natl. Acad. Sci. USA, 118, 1–7, https://doi.org/10.1073/pnas.2015797118, 2021.

Li, M., Yu, S., Chen, X., Li, Z., Zhang, Y., Wang, L., Liu, W., Li, P., Lichtfouse, E., Rosenfeld, D., and Seinfeld, J. H.: Large scale control of surface ozone by relative humidity observed during warm seasons in China, Environ. Chem. Lett., 19, 3981–3989, https://doi.org/10.1007/s10311-021-01265-0, 2021a.

Li, M., Wang, T., Shu, L., Qu, Y., Xie, M., Liu, J., Wu, H., and Kalsoom, U.: Rising surface ozone in China from 2013 to 2017: A response to the recent atmospheric warming or pollutant controls?, Atmos. Environ., 246, 118130, https://doi.org/10.1016/j.atmosenv.2020.118130, 2021b.

Lin, J.-T., and McElroy, M. B.: Impacts of boundary layer mixing on pollutant vertical profiles in the lower troposphere: Implications to satellite remote sensing, Atmos. Environ., 44, 1726–1739, https://doi.org/10.1016/j.atmosenv.2010.02.009, 2010.

Liu, R., Ma, Z., Liu, Y., Shao, Y., Zhao, W., and Bi, J.: Spatiotemporal distributions of surface ozone levels in China from 2005 to 2017: a machine learning approach, Environ. Int., 142, 105823, https://doi.org/10.1016/j.envint.2020.105823, 2020.

Liu, S., Xing, J., Zhang, H., Ding, D., Zhang, F., Zhao, B., Sahu, S. K., and Wang, S.: Climate-driven trends of biogenic volatile organic compound emissions and their impacts on summertime ozone and secondary organic aerosol in China in the 2050s, Atmos. Environ., 218, 117020, https://doi.org/10.1016/j.atmosenv.2019.117020, 2019.

Liu, X., Zhu, Y., Xue, L., Desai, A. R., and Wang, H.: Cluster-enhanced ensemble learning for mapping global monthly surface ozone from 2003 to 2019, Geophys. Res. Lett., 49, e2022GL097947, https://doi.org/10.1029/2022GL097947, 2022.

Liu, Y., and Wang, T.: Worsening urban ozone pollution in China from 2013 to 2017–Part 1: The complex and varying roles of meteorology, Atmos. Chem. Phys., 20, 6305–6321, https://doi.org/10.5194/acp-20-6305-2020, 2020.

Lou, S., Liao, H., and Zhu, B.: Impacts of aerosols on surface-layer ozone concentrations in China through heterogeneous reactions and changes in photolysis rates, Atmos. Environ., 85, 123–138, http://dx.doi.org/10.1016/j.atmosenv.2013.12.004, 2014.

Lu, X., Zhang, L., Chen, Y., Zhou, M., Zheng, B., Li, K., Liu, Y., Lin, J., Fu, T.-M., and Zhang, Q.: Exploring 2016–2017 surface ozone pollution over China: source contributions and meteorological influences, Atmos. Chem. Phys., 19, 8339–8361, https://doi.org/10.5194/acp-19-8339-2019, 2019.

Lu, X., Zhang, L., Wang, X., Gao, M., Li, K., Zhang, Y., Yue, X., and Zhang, Y.: Rapid Increases in Warm-Season Surface Ozone and Resulting Health Impact in China since 2013, Environ. Sci. Technol. Lett., 7, 240–247, https://doi.org/10.1021/acs.estlett.0c00171, 2020.

Malley, C. S., Henze, D. K., Kuylenstierna, J. C. I., Vallack, H., Davila, Y., Anenberg, S. C., Turner, M. C., and Ashmore, M.: Updated Global Estimates of Respiratory Mortality in Adults ≥ 30 Years of Age Attributable to Long-Term Ozone Exposure, Environ. Health Perspect., 125, 087021, https://doi.org/10.1289/EHP1390, 2017.

Mao, J., Paulot, F., Jacob, D. J., Cohen, R. C., Crounse, J. D., Wennberg, P. O., Keller, C. A., Hudman, R. C., Barkley, M. P., and Horowitz, L. W.: Ozone and organic nitrates over the eastern United States: sensitivity to isoprene chemistry, J. Geophys. Res. Atmos, 118, 11256–68, https://doi.org/10.1002/jgrd.50817, 2013.

Marvin, M. R., Palmer, P. I., Latter, B. G., Siddans, R., Kerridge, B. J., Latif, M. T., and Khan, M. F.: Photochemical environment over Southeast Asia primed for hazardous ozone levels with influx of nitrogen oxides from seasonal biomass burning, Atmos. Chem. Phys., 21, 1917–1935, https://doi.org/10.5194/acp-21-1917-2021, 2021.

McLinden, C. A., Olsen, S. C., Hannegan, B., Wild, O., Prather, M. J., and Sundet, J.: Stratospheric ozone in 3-D models: A simple chemistry and the

cross-tropopause flux, J. Geophys. Res. Atmos., 105, 14653–14665, https://doi.org/10.1029/2000jd900124, 2000.

Mills, G., Pleijel, H., Malley, C. S., Sinha, B., Cooper, O. R., Schultz, M. G., Neufeld, H. S., Simpson, D., Sharps, K., Feng, Z., Gerosa, G., Harmens, H., Kobayashi, K., Saxena, P., Paoletti, E., Sinha, V., and Xu, X.: Tropospheric ozone assessment report: Present-day tropospheric ozone distribution and trends relevant to vegetation, Elem. Sci. Anth., 6, 47, https://doi.org/10.1525/elementa.302, 2018.

Murray, L. T., Jacob, D. J., Logan, J. A., Hudman, R. C., and Koshak, W. J.: Optimized regional and interannual variability of lightning in a global chemical transport model constrained by LIS/OTD satellite data, J. Geophys. Res. Atmos., D20307, https://doi.org/10.1029/2012jd017934, 2012.

Ni, R., Lin, J., Yan, Y., and Lin, W.: Foreign and domestic contributions to springtime ozone over China, Atmos. Chem. Phys., 18, 11447–11469, https://doi.org/10.5194/acp-18-11447-2018, 2018.

O'Neill, B. C., Tebaldi, C., van Vuuren, D. P., Eyring, V., Friedlingstein, P., Hurtt, G., Knutti, R., Kriegler, E., Lamarque, J.-F., Lowe, J., Meehl, G. A., Moss, R., Riahi, K., and Sanderson, B. M.: The Scenario Model Intercomparison Project (ScenarioMIP) for CMIP6, Geosci. Model Dev., 9, 3461–3482, https://doi.org/10.5194/gmd-9-3461-2016, 2016.

Ott, L. E., Pickering, K. E., Stenchikov, G. L., Allen, D. J., DeCaria, A. J., Ridley, B., Lin, R.-F., Lang, S., and Tao, W.-K.: Production of lightning NO_x and its vertical distribution calculated from three-dimensional cloud-scale chemical transport model simulations, J. Geophys. Res., 115, D04301, https://doi.org/10.1029/2009JD011880, 2010.

Park, R. J., Jacob, D. J., Field, B. D., Yantosca, R. M., and Chin, M.: Natural and transboundary pollution influences on sulfate-nitrate-ammonium aerosols in the United States: Implications for policy, J. Geophys. Res. Atmos., 109, 20, https://doi.org/10.1029/2003jd004473, 2004.

Ploton, P., Mortier, F., Réjou-Méchain, M., Barbier, N., Picard, N., Rossi, V., Dormann, C., Cornu, G., Viennois, G., Bayol, N., Lyapustin, A., Gourlet-Fleury, S., and Pélissier, R.: Spatial validation reveals poor predictive performance of large-scale ecological mapping models, Nat. Commun., 11, 1–11, https://doi.org/10.1038/s41467-020-18321-y, 2020.

Pommier, M., Fagerli, H., Gauss, M., Simpson, D., Sharma, S., Sinha, V.,

Ghude, D. S., Landgren, O., Nyiri, A., and Wind, P.: Impact of regional climate change and future emission scenarios on surface O_3 and $PM_{2.5}$ over India, Atmos. Chem. Phys., 18, 103–27, https://doi.org/10.5194/acp-18-103-2018, 2018.

Pye, H. O. T., Liao, H., Wu, S., Mickley, L. J., Jacob, D. J., Henze, D. K., and Seinfeld, J. H.: Effect of changes in climate and emissions on future sulfate-nitrate-ammonium aerosol levels in the United States, J. Geophys. Res. Atmos., 114, D01205, https://doi.org/10.1029/2008jd010701, 2009.

Qian, J., Liao, H., Yang, Y., Li, K., Chen, L., and Zhu, J.: Meteorological influences on daily variation and trend of summertime surface ozone over years of 2015–2020: Quantification for cities in the Yangtze River Delta, Sci. Total Environ., 834, 155107, https://doi.org/10.1016/j.scitotenv.2022.155107, 2022.

Rodriguez, J. D., Perez, A., and Lozano, J. A.: Sensitivity analysis of k-fold cross validation in prediction error estimation, IEEE T. Pattern Anal., 32, 569–575, https://doi.org/10.1109/TPAMI.2009.187, 2010.

Santurtún, A., González-Hidalgo, J. C., Sanchez-Lorenzo, A., and Zarrabeitia, M. T.: Surface ozone concentration trends and its relationship with weather types in Spain (2001–2010), Atmos. Environ., 101, 10–22, https://doi.org/10.1016/j.atmosenv.2014.11.005, 2015.

Su, X., An, J., Zhang, Y., Zhu, P., and Zhu, B.: Prediction of ozone hourly concentrations by support vector machine and kernel extreme learning machine using wavelet transformation and partial least squares methods, Atmos. Pollut. Res., 6, 51–60, https://doi.org/10.1016/j.apr.2020.02.024, 2020.

Toh, Y. Y., Lim, S. F., and von Glasow, R.: The influence of meteorological factors and biomass burning on surface ozone concentrations at Tanah Rata, Malaysia, Atmos. Environ., 70, 435–446, https://doi.org/10.1016/j.atmosenv.2013.01.018, 2013.

van der Werf, G. R., Randerson, J. T., Giglio, L., van Leeuwen, T. T., Chen, Y., Rogers, B. M., Mu, M., van Marle, M. J. E., Morton, D. C., Collatz, G. J., Yokelson, R. J., and Kasibhatla, P. S.: Global fire emissions estimates during 1997–2016, Earth Syst. Sci. Data, 9, 697–720, https://doi.org/10.5194/essd-9-697-2017, 2017.

Wang, Y., Shen, L., Wu, S., Mickley, L. J., He, J., and Hao, J.: Sensitivity of surface ozone over China to 2000–2050 global changes of climate and

emissions, Atmos. Environ., 75, 374–382, https://doi.org/10.1016/j.atmosenv.2013.04.045, 2013.

Wang, Z., Lin, L., Xu, Y., Che, H., Zhang, X., Dong, W., Wang, C., Gui, K., and Xie, B.: Incorrect Asian aerosols affecting the attribution and projection of regional climate change in CMIP6 models, npj Clim. Atmos. Sci., 4, 2, https://doi.org/10.1038/s41612-020-00159-2, 2021.

Wei, J., Li, Z., Li, K., Dickerson, R., Pinker, R., Wang, J., Liu, X., Sun, L., Xue, W., and Cribb, M.: Full-coverage mapping and spatiotemporal variations of ground-level ozone (O_3) pollution from 2013 to 2020 across China, Remote Sens. Environ., 270, 112775, https://doi.org/10.1016/j.rse.2, 2022.

Weng, X., Forster, G. L., and Nowack, P.: A machine learning approach to quantify meteorological drivers of ozone pollution in China from 2015 to 2019, Atmos. Chem. Phys., 22, 8385–8402, https://doi.org/10.5194/acp-22-8385-2022, 2022.

Xu, Z., Han, Y., Tam, C. Y., Yang, Z., and Fu, C.: Bias-corrected CMIP6 global dataset for dynamical downscaling of the historical and future climate (1979–2100), Sci. Data, 8, 293, https://doi.org/10.1038/s41597-021-01079-3, 2021.

Xue, T., Zheng, Y., Geng, G., Xiao, Q., Meng, X., Wang, M., Li, X., Wu, N., Zhang, Q., and Zhu, T.: Estimating Spatiotemporal Variation in Ambient Ozone Exposure during 2013–2017 Using a Data-Fusion Model, Environ. Sci. Technol., 54, 14877–14888, https://dx.doi.org/10.1021/acs.est.0c03098, 2020.

Yang, Y., Li, M., Wang, H., Li, H., Wang, P., Li, K., Gao, M., and Liao, H.: ENSO modulation of summertime tropospheric ozone over China, Environ. Res. Lett., 17, 034020, https://doi.org/10.1088/1748-9326/ac54cd, 2022.

Yin, Z., Cao, B., and Wang, H.: Dominant patterns of summer ozone pollution in eastern China and associated atmospheric circulations, Atmos. Chem. Phys., 19, 13933–13943, https://doi.org/10.5194/acp-19-13933-2019, 2019.

Yue, X., Unger, N., Harper, K., Xia, X., Liao, H., Zhu, T., Xiao, J., Feng, Z., and Li, J.: Ozone and haze pollution weakens net primary productivity in China, Atmos. Chem. Phys., 17, 6073–6089, https://doi.org/10.5194/acp-17-6073-2017, 2017.

Zanis, P., Akritidis, D., Turnock, S., Naik, V., Szopa, S., Georgoulias, A. K., Bauer, S. E., Deushi, M., Horowitz, L. W., Keeble, J., Le Sager, P.,

O'Connor, F. M., Oshima, N., Tsigaridis, K., and van Noije., T.: Climate change penalty and benefit on surface ozone: a global perspective based on CMIP6 earth system models, Environ. Res. Lett., 17, 024014, https://doi.org/10.1088/1748-9326/ac4a34, 2022.

Zhang, X., Zhao, L., Cheng, M., and Chen, D.: Estimating ground-level ozone concentrations in eastern China using satellite-based precursors, IEEE Trans. Geosci. Remote Sens., 58, 4754–4763, https://doi.org/10.1109/TGRS.2020.2966780, 2020.

Zhou, C., Gao, M., Li, J., Bai, K., Tang, X., Lu, X., Liu, C., Wang, Z., and Guo, Y.: Optimal Planning of Air Quality-Monitoring Sites for Better Depiction of $PM_{2.5}$ Pollution across China, Environ. Au., 2, 314–323, https://doi.org/10.1021/acsenvironau.1c00051, 2022.

Zhu, J., Liao, H., Mao, Y., Yang, Y., and Jiang, H.: Interannual variation, decadal trend, and future change in ozone outflow from East Asia, Atmos. Chem. Phys., 17, 3729–3747, https://doi.org/10.5194/acp-17-3729-2017, 2017.

930 **Table 1.** Summary of detailed datasets used in this study.

Dataset type	Variable	Description	Spatial resolution	Temporal resolution	Time period	Data source
O_3	O_3	Near-surface ozone concentrations	0.5°×0.625°	Monthly (historical)	2014–2019 (historical)	Assimilated GEOS-Chem simulations and Observations
Meteorology	T_2m	Air temperature at 2 meters	0.5°×0.625°	Monthly (historical) Monthly (future)	2014–2019 (historical) 2020–2100 (future)	MERRA-2 (historical) Adjusted CMIP6 (future)
	T_850	Air temperature at 850 hPa				
	T_500	Air temperature at 500 hPa				
	U_850	Zonal wind at 850 hPa				
	U_500	Zonal wind at 500 hPa				
	V_850	Meridional wind at 850 hPa				
	V_500	Meridional wind at 500 hPa				
	RH	Relative humidity				
	PRECP	Precipitation rate				
	CLT	Total cloud cover				
	RSDS	Incoming shortwave radiation at the surface				
	SLP	Sea level pressure				
Emission	NO_x	Nitric oxide from anthropogenic sources	0.5°×0.625°	Monthly (historical) Monthly (future)	2014–2019 (historical) 2019 (future)	CEDS (Anthropogenic) GFED4 (Biomass burning) MEGAN V-2.1 (Biogenic)
		Nitric oxide from biomass burning				
		Nitric oxide from soil sources			2016	
		Nitric oxide from lightning sources			2016	
	CO	Carbon monoxide from anthropogenic sources			2014–2019 (historical) 2019 (future)	
		Carbon monoxide from biomass burning				
	NMVOC	Non-methane volatile organic compounds from anthropogenic sources				
		Non-methane volatile organic compounds from biomass burning				
		Non-methane volatile organic compounds from biogenic sources			2016	
Land use	LC	Land cover	300 m×300 m	Monthly	2014–2019 (historical) 2019 (future)	ESA CCI AVHRR
	NDVI	Normalized Difference Vegetation Index	0.05°×0.05°			
Topography	TOPO	Digital elevation model	90 m×90 m	-	2010	SRTM
Population	POP	Population density	1 km×1 km	-	2010	Land Scan

931

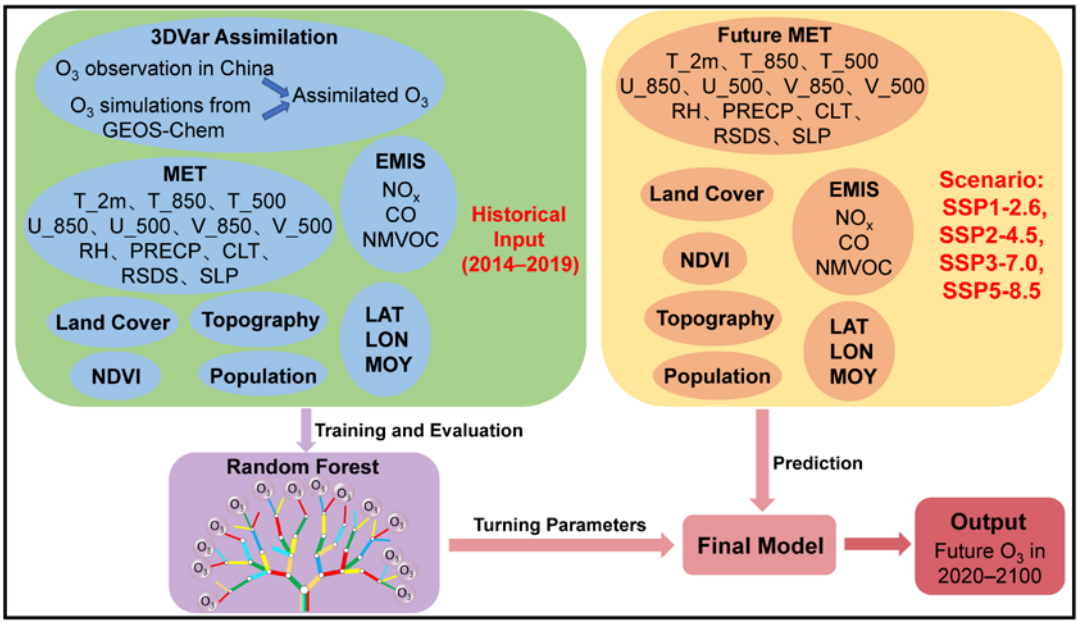

Figure 1. The structure and specific schematics for predicting future O_3 concentrations under four scenarios based on the machine learning (ML) method.

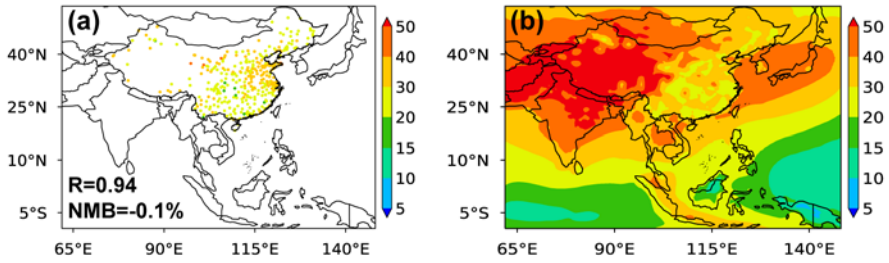

Figure 2. Spatial distributions of observed near-surface O_3 concentrations across China (a) and assimilated O_3 concentrations over Asia (b) in 2014–2019. Correlation coefficient (R) between observed and assimilated O_3 and the normalized mean bias (NMB = ∑ (Observed – Assimilated) / ∑Assimilated × 100%) are given at the bottom left of panel (a).

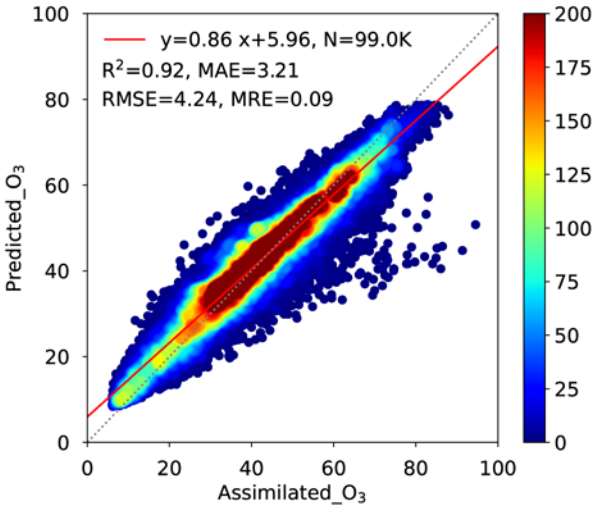

Figure 3. Density scatterplots of predicted vs assimilated monthly near-surface O_3 concentrations (ppb) in 2019 over Asia. The gray and red lines are the 1:1 line and linear regression line, respectively. Statistical metrics including the number of samples (N), correlation of determination (R^2, unitless), root mean square error (RMSE, ppb), mean absolute error (MAE, ppb), and mean relative error (MRE, %) are shown at the top left.

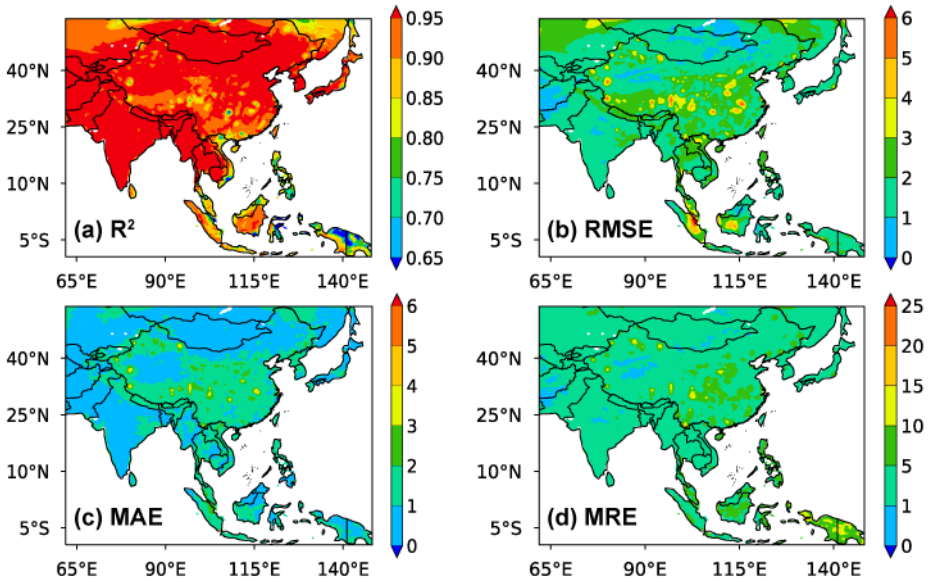

Figure 4. Spatial distributions of the performance statistics of the ML model with regard to (a) R^2 (unitless), (b) RMSE (ppb), (c) MAE (ppb), and (d) MRE (%) during 2014–2019 over Asia.

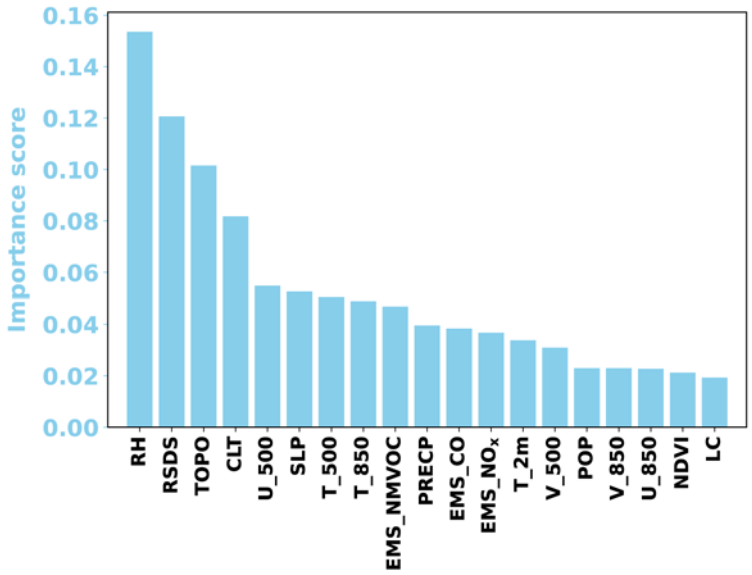

Figure 5. Importance scores of independent variables (meteorological parameters, emissions, land use, topography, and population density) used in the ML model for predicting future near-surface O_3 concentrations over Asia.

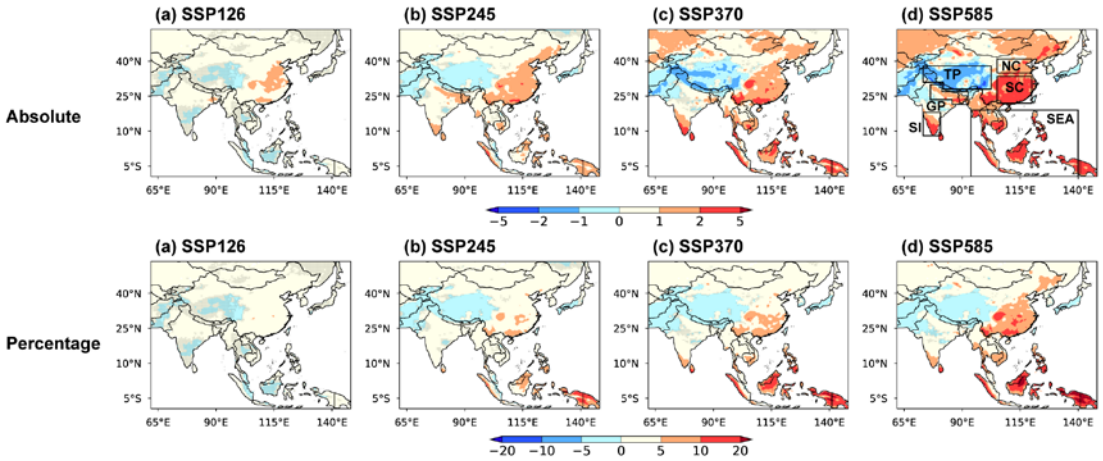

Figure 6. The spatial distributions of absolute (ppb) and percentage difference (%) of surface O_3 level between 2025 (2020–2029 mean) and 2095 (2091–2100 mean) driven by climate change under four scenarios (a, e) SSP1-2.6, (b, f) SSP2-4.5, (c, g) SSP3-7.0 and (d, h) SSP5-8.5. The box-outlined areas in (d) are North China (NC, 35°–41°N, 105°–120°E), South China (SC, 22°–33.5°N, 105°–120°E), Southeast Asia (SEA, -9.5°S–19°N, 93.75°–140°E), South India (SI, 8°–18°N, 73.125°–80.625°E), Gangetic Plains (GP, 21.5°–23.5°N, 85.625°–92.5°E, 23.5°–27°N, 76.25°–92.5°E, and 27°–30°N, 76.25°–81.25°E), and Tibetan Plateau (TP, 28°–31°N, 81.875°–102.5°E and 31°–38°N, 73.125°–102.5°E). No overlaying hatch pattern indicates statistical significance with 95% confidence from a two-tailed t test.

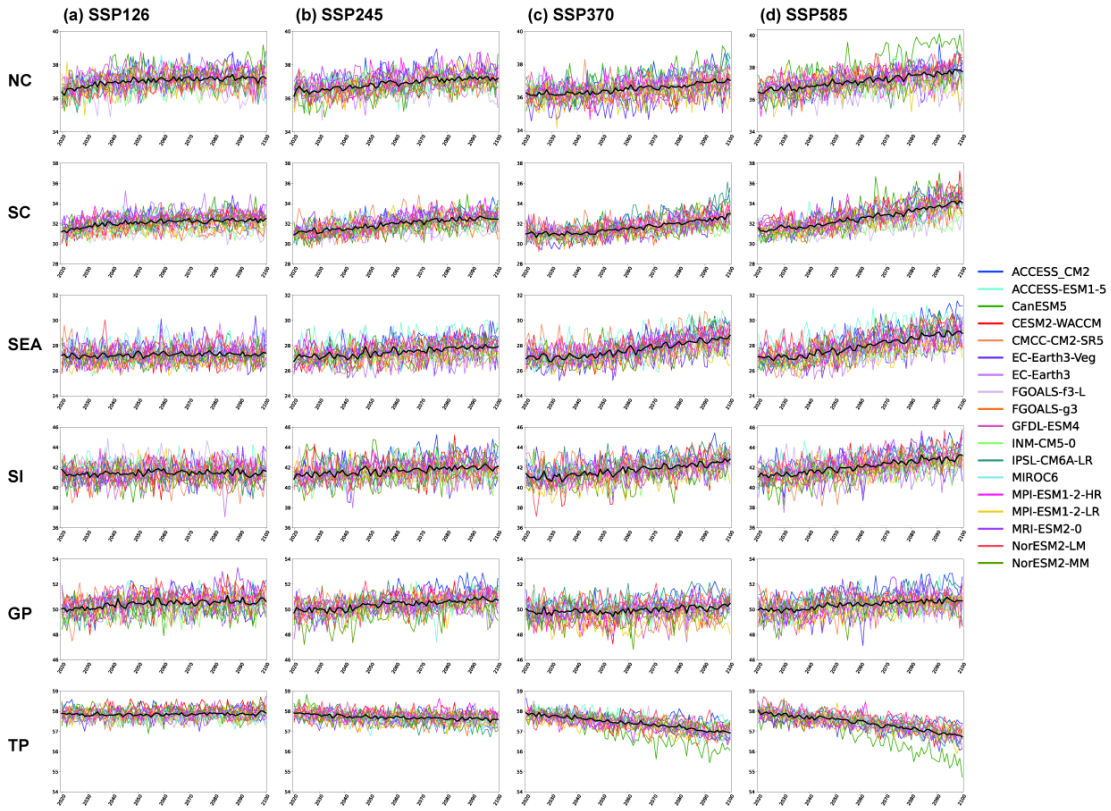

Figure 7. Time series (2020–2100) of annual mean near-surface O_3 concentrations (ppb) driven by climate change under the four scenarios (SSP1-2.6, SSP2-4.5, SSP3-7.0 and SSP5-8.5) over North China (NC, 35°–41°N, 105°–120°E), South China (SC, 22°–33.5°N, 105°–120°E), Southeast Asia (SEA, -9.5°S–19°N, 93.75°–140°E), South India (SI, 8°–18°N, 73.125°–80.625°E), Gangetic Plains (GP, 21.5°–23.5°N, 85.625°–92.5°E, 23.5°–27°N, 76.25°–92.5°E, and 27°–30°N, 76.25°–81.25°E), and Tibetan Plateau (TP, 28°–31°N, 81.875°–102.5°E and 31°–38°N, 73.125°–102.5°E). The black lines are the averages of the predicted O_3 based on meteorological fields from 18 CMIP6 models.

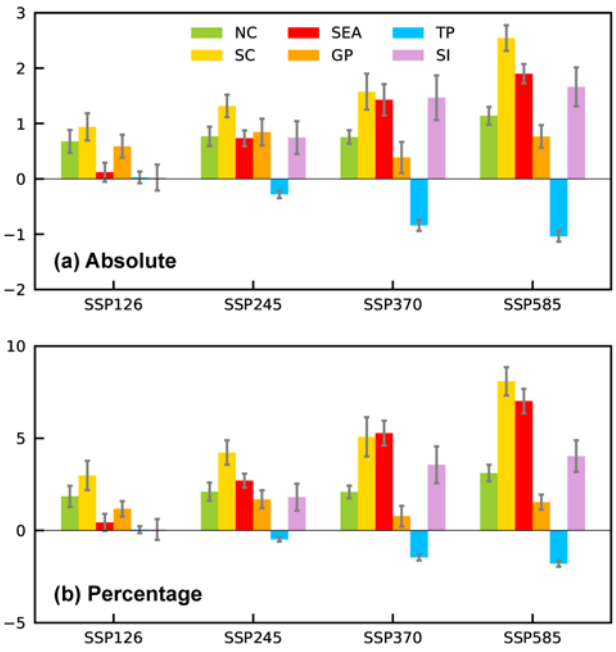

Figure 8. Absolute (a, ppb) and percentage (b, %) changes in projected near-surface climate-driven O_3 concentrations in 2095 (2091–2100 mean) relative to 2025 (2020–2029 mean) over the six selected key regions of Asia, including NC, SC, SEA, SI, GP, and TP under four future climate scenarios. The error bars indicate one standard deviation.

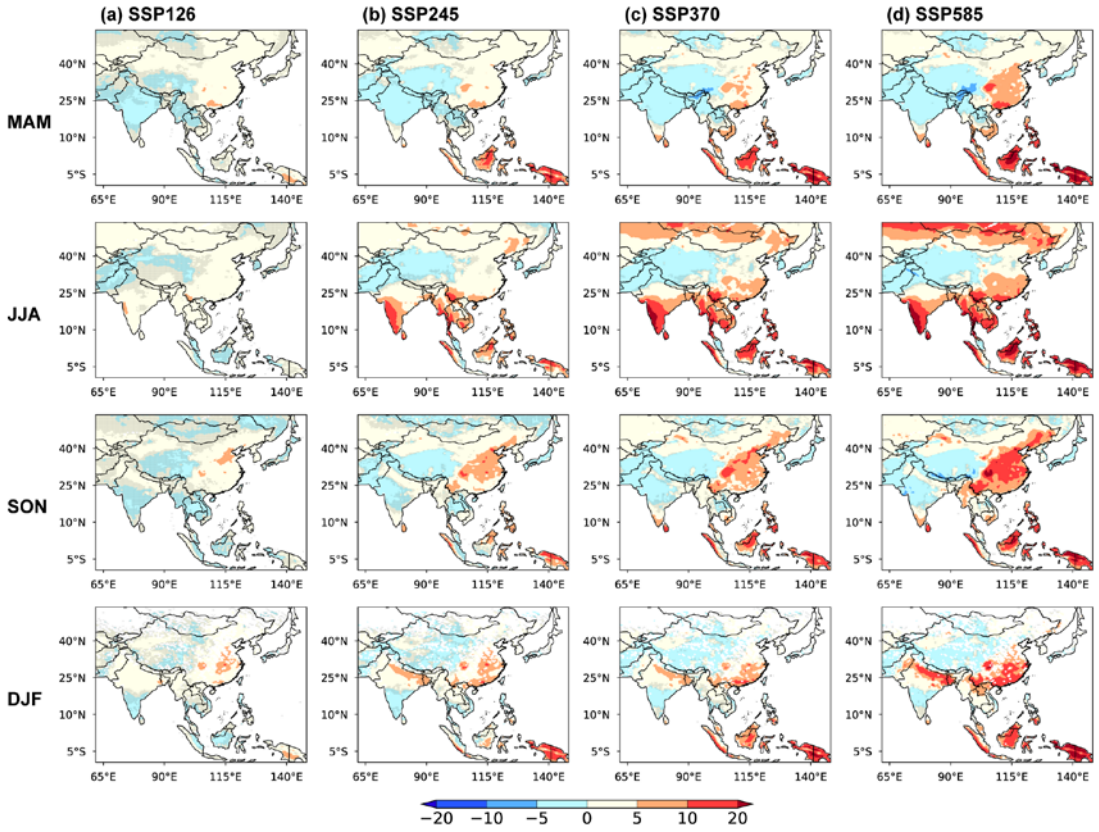

Figure 9. The spatial distributions of percentage differences (%) in near-surface O_3 concentrations between 2025 (2020–2029 mean) and 2095 (2091–2100 mean) driven by climate change under four scenarios (SSP1-2.6, SSP2-4.5, SSP3-7.0 and SSP5-8.5, from left to right) averaged in MAM (March–April–May), JJA (June–July–August), SON (September–October–November), and DJF (December–January–February) (from top to bottom). No overlaying hatch pattern indicates statistical significance with 95% confidence from a two-tailed t test.